Phase slippage driven dissipation and high-field Little-Parks effect in superconducting MoGe nanowire networks formed on nanoporous substrates

Q. Luo, X. Q. Zeng, M. E. Miszczak, Z. L. Xiao, J. Pearson, T. Xu, and W. K. Kwok

Phys. Rev. B **85**, 174513 — Published 14 May 2012

DOI: 10.1103/PhysRevB.85.174513

Phase slippage driven dissipation and high field Little-Parks effect in superconducting MoGe nanowire networks formed on nanoporous substrates

Q. Luo[1], X. Q. Zeng[2,3], M. E. Miszczak[1], Z. L. Xiao*[1, 2], J. Pearson[2], T. Xu[2,3], and W. K. Kwok[2]

[1]Department of Physics, Northern Illinois University, DeKalb, Illinois 60115

[2]Materials Science Division, Argonne National Laboratory, Argonne, Illinois 60439

[3]Department of Chemistry and Biochemistry, Northern Illinois University, DeKalb, Illinois 60115

Superconducting MoGe nanowires with extremely small transverse dimensions have served as unique platforms for exploring physical phenomena in one-dimensional (1D) superconductors. Here we report on networks of superconducting MoGe nanowires with transverse dimensions down to a few nanometers, fabricated by sputter-deposition of MoGe onto commercially available filtration membranes containing dense nanopores. These networks of nanowires exhibit physical properties of individual MoGe nanowires, such as thermally activated phase slips – a dissipation mechanism expected for 1D superconducting nanowires. Furthermore, anomalies in the magnetic field versus temperature phase diagram around 1.2-1.5 Tesla and in the magnetoresistance curves can be understood with the Little-Parks effect, consistent with the multiply connected nature of a network of 1D nanowires.

PACS numbers: 74.50.+r, 74.45.+c, 74.78.Na

I. INTRODUCTION

One of the characteristic properties of a bulk superconductor is its ability to conduct electricity without resistance, i.e., no energy dissipation.[1] With reduction of its dimensions, however, a superconductor can be resistive over a wide temperature range[2-11] or even become insulating.[2-5] Superconducting nanowires have been the subject of intensive research because they provide unique platforms to explore the dissipation mechanisms and to discover new phenomena in a confined geometry.[2-26] When the nanowire's transverse dimensions are comparable to its superconducting coherence length ξ, only one channel is available for the supercurrent. Fluctuations of the order parameter $\Psi = |\Psi| \exp(i\varphi)$ result in a temporary local destruction of $|\Psi|$ accompanied by a phase slippage and destroy the phase coherence in the wire. According to the Josephson relation $V = \dot{\varphi}/2e$ the phase slippage results in a momentary voltage V at the corresponding point.[27,28] These instant voltage jumps, integrated in time, result in a nonzero voltage across the superconducting nanowire, thus bringing it into a resistive state. Two different scenarios have been developed to describe the rate of fluctuation of the order parameter (phase slips) in 1D superconducting nanowires: thermally activated phase slips (TAPS)[29,30] and quantum phase slips (QPS).[31] The principal difference is that in TAPS, the required energy for the fluctuation is provided by the 'classical' temperature term $\sim k_B T$, while in QPS the relevant energy scale is $\sim h\Gamma_{QPS}$ where k_B and h are the Boltzman and Planck constants, respectively, and Γ_{QPS} is the QPS rate.[28]

Early experiments exploring the phase slip phenomena were conducted in tin (Sn) nanowires nearly forty years ago.[32] However, due to the limitation in the smallest transverse dimensions achievable at that time, the samples displayed 1D behavior only within a narrow temperature range of a few mK below the zero-field critical temperature T_{c0}, allowing experimental verification of

only the TAPS model. In recent years, significant progress has been achieved in fabricating superconducting nanowires with transverse dimensions down to tens of nanometers or even a few nanometers.[4,5,24,25] New phenomena such as negative magnetoresistance[13,14] and magnetic field enhanced superconductivity[33] have been observed in these ultra-small nanowires. Furthermore, they exhibit broad superconducting transitions, enabling possible observation of QPS induced dissipation.[2-6,24-26]. Although a long resistance tail in the $R(T)$ curve has been often associated with manifestation of the QPS mechanism, interpretation of these results can be flawed by the presence of granularity in the nanowires that could give rise to a similar temperature dependence of the resistance.[8,11] Thus, it is crucial to achieve homogeneous ultra-small nanowires for revealing quantum phase slip related phenomena.

Currently, the most promising way to fabricate ultra-small nanowires is with molecular templating[25], which involves the sputter-deposition of a thin superconducting layer over a carbon nanotube (or nanotube bundle) or a DNA molecule suspended over a specially designed nanoscale trench. The templating approach is desirable for fabricating high-quality clean nanostructures since it eliminates nanofabrication processes such as etching, releasing nanowires from nanopores, and nanocontacting, which can result in sample damage and degradation. For example, amorphous superconducting MoGe nanowires produced via molecular templating are homogeneous and can be fabricated with transverse dimensions less than 10 nm. They have been investigated extensively for exploring both TAPS and QPS phenomena.[25]

Recently, we demonstrated a template nanofabrication approach[34] that can produce samples with the physical and chemical properties of single nanowires: networks of palladium (Pd) nanowires with ultra-small transverse dimensions were achieved by sputter-depositing palladium onto nanoporous substrates[35] which are commercially available and inexpensive. The performance

of these nanowire networks on hydrogen gas sensing was found to outperform individual Pd nanowires. They also served as convenient platforms for investigating confinement phenomena such as size effects on phase transitions in Pd/H system.[36]

Here, we report on results utilizing the above method to produce superconducting samples to investigate dissipation associated with phase-slip phenomena. We sputter-deposited a thin layer of superconducting amorphous MoGe, onto commercially available filtration membranes which contain extremely dense nanopores, enabling the formation of a network of superconducting MoGe nanowires with transverse dimensions down to a few nanometers. Resistive dissipation of these superconducting samples can be attributed to the TAPS mechanism, though we were unable to explore QPS phenomena below 2 K due to the limitations of our cryogenic system. Our network of superconducting MoGe nanowires, which can be obtained rather conveniently, exhibit physical properties expected of individual MoGe nanowires with ultra-small transverse dimensions and provide a new system for investigating phase slips and other phenomena in confined superconducting structures. Furthermore, the multiply connected nature of our nanowire network makes them resemble a network of superconducting loops – the model system in which Little[37] first proposed phase-slips to understand the decay in supercurrent. Such networks with average hole diameters of 10-20 nm can be used to investigate the Little-Parks depression of the superconducting critical temperature to T = 0 K, inducing a field-driven quantum phase transition from superconducting to metallic or insulating.[38] In our MoGe nanowire networks, we observed a minimum in the magnetoresistance at a field value as high as 1.2-1.5 Tesla, originating from the Little-Parks effect.

II. EXPERIMENT

Porous Anodisc® inorganic membranes from Whatman® Company[35] have been widely used as filters in chemistry. Though the available nominal effective filtration pore diameters are 20 nm, 50 nm, 100 nm, and 200 nm, on the surface, the diameter of the nanochannels in the bulk of the membrane is unchanged (i.e. 200 nm).[35] The effective filtration of the membranes with pore diameter smaller than 200 nm is determined by the pore diameters of a very thin (~300-400 nm) layer of a nano-porous network array supported on top of a 60 μm thick membrane containing vertical nanochannels of 200 nm in diameter, as shown by the schematic given in the inset of Fig.4(a) in Ref.35 and the cross-section micrograph given in inset of Fig.1(a) in Ref.34. For a nominal effective filtration pore diameter of 20 nm, the material sections between neighboring pores is less than 10 nm wide [please see Fig.4(b) in Ref.35 for a micrograph on the surface of a bare membrane]. We utilized these sections as templates to form a superconducting wire network array by depositing MoGe onto them.

Anodisc®13 membranes with a nominal filtration pore diameter of 20 nm were cleaned in acetone for 10 mins in an ultrasonic bath and then rinsed with de-ionized water followed with an ethanol rinse. They were dried using high-purity nitrogen gas.[34,36] MoGe layers with thicknesses of 6, 10, 15 and 20 nm were sputtered onto the filtration membranes from a two inch diameter $Mo_{0.79}Ge_{0.21}$ alloy target (AJA International, USA) . The elemental composition of the alloy was optimized for achieving the highest critical temperature for the superconducting transition and have been previously used in fabricating ultra-small MoGe nanowires through molecular templating.[25] A reference film with a spacing of 200 μm between voltage contacts was prepared for each nanowire network sample by placing a silicon substrate (with an oxide top layer of 300 nm and with lithographically patterned microbridge of 50 μm wide) next to the Anodisc membranes during sputtering. The deposition system has a base pressure of $2x10^{-7}$ Torr and the argon-gas working

pressure was maintained at 3 mTorr during the sputtering. The deposition rate was 1.3 Å/s, determined by an in-situ quartz crystal microbalance (QCM) thickness monitor (model TM-350 from Maxtek, Inc.). The sputtering time was determined from the desired nominal thickness divided by the deposition rate. A high-resolution field emission scanning electron microscope (FESEM) (Hitachi S-4700II) was used to image the morphology of the fabricated samples. The samples were mounted onto an aluminum holder with double-sided carbon tape. The top surface of the MoGe coated sample was also connected to the sample holder with double-sided carbon tape to avoid charging effects during imaging. For resistivity measurements, a rectangular sample of ~1.5 mm wide was first cut from the MoGe coated Anodisc membrane with a razor blade. Then four gold wires of 50 μm in diameter were attached to the MoGe coated surface with silver paste. The distances between the two voltage-contacts were ~2.5 mm. The resistance of the sample was measured using a standard four-probe dc method with a Physical Property Measurement System (PPMS-9, Quantum Design, Inc). The sample was placed on a stepper-controlled horizontal rotator with a rotation range of -10° to 370° and with an angular resolution of 0.05°, enabling the alignment of the magnetic field perpendicular to the sample surface ($\theta = 0°$) and the exploration of the angular dependence of the magnetoresistance $R(\theta)$. The temperature dependence of the resistivity, $R(T)$, in fixed applied magnetic fields was measured with a cooling rate of 50 mK/min. The field dependence of the resistivity $R(H)$ and the current-voltage (I-V) characteristics were measured at fixed temperatures with a temperature stability of 1 mK.

III. RESULTS AND DISCUSSION

Figure 1 (a), (b), (c) and (d) present top-view SEM micrographs of Anodisc® 13 membranes with a nominal pore diameter of 20 nm after depositing MoGe layers with nominal thicknesses of 6 nm (sample A), 10 nm (sample B), 15 nm (sample C), and 20 nm (sample D), respectively. Comparing

with the image presented in Fig.4(b) of Ref.35, one finds that the morphology of the samples coated with 6 nm and 10 nm thick MoGe layers (Fig.1 (a) and (b)), does not change significantly from that of the bare filtration membrane. That is, the diameter of the holes in the MoGe layer is the same as those of the pores in the filtration membrane substrate. By increasing the thickness of the deposited MoGe layer, the hole size shrinks and the width of the MoGe sections between neighboring holes becomes larger, as can be seen from the micrograph presented in Fig.1(d). Quantitatively, the widths of the MoGe nanowires (ie. sections between neighboring holes) change from 7-9 nm (sample A) to 12-15 nm (sample D) when the thickness of the deposited MoGe layer increases from 6 nm to 20 nm, respectively. Cross-section SEM imaging also reveals that there is no identifiable MoGe coating on the inner walls of the pores in the membrane. This is understandable, since in magnetron sputtering the deposited material is emitted from a ring of ~5 mm in width close to the edge of our 2 inch diameter target. Hence it is unlikely that the sputtered materials can enter into the pores of only ~20 nm in diameter, located 5 inches away from the target. Furthermore, results of our resistivity measurements will not be affected even if there were a discontinuous thin layer coating the inner walls of the nanopores.

A quantitative description of the dissipation induced by TAPS in a 1D superconducting wire was first developed by Langer and Ambergaokar,[29] and by McCumber and Halperin.[30] The LAMH theory predicts a TAPS rate of [27]

$$\Gamma = \frac{4\sqrt{6}}{\sqrt{\pi}} T^* \frac{L}{\xi(T)} \sqrt{\frac{\Delta(T)}{T}} \exp\left[-\frac{\Delta(T)}{T}\right] \qquad (1)$$

where T^* is an effective crossover temperature between the thermal activation regime and that of quantum tunneling regime. L is the length of the wire, and $\xi(T) = \xi_0(1 - T/T_{c0})^{-1/2}$ is the temperature dependent superconducting coherence length with ξ_0, the value at zero temperature.

$\Delta(T) = \Delta(0)(T_{c0} - T)^{3/2}$ is the temperature dependent effective energy barrier at the low current limit.

In the presence of a small bias current I ($<< I_c$) and at temperatures near T_{c0} the TAPS will result in a voltage V across the wire:[27]

$$V = \frac{2\pi}{e}\Gamma \sinh\frac{\pi I}{2eT} \tag{2}$$

This leads to an exponential dependence on temperature for the zero-bias resistance $R(T) = (\partial V / \partial I)_{I=0}$:[27]

$$R(T) = \frac{4\sqrt{6}\pi^{3/2}}{e^2}\frac{T^*}{T}\frac{L}{\xi(T)}\sqrt{\frac{\Delta(T)}{T}}\exp\left[-\frac{\Delta(T)}{T}\right] \tag{3}$$

Though Equations (2) and (3) were derived for an individual superconducting nanowire, we found that they can also describe the dissipation in our samples. Figure 2(a) presents voltage versus current $V(I)$ curves for sample D which has the largest nominal MoGe layer thickness, i.e. the widest superconducting sections between neighboring holes. The $V(I)$ curves display Ohmic behavior at small currents and nonlinearity sets in with increasing current. The solid lines are fits to the data using Eq.(2) and match the experimental data very well. Comparisons between the theoretical temperature dependence of the TAPS induced resistance Eq.(3) and the measured $R(T)$ curves are presented in Fig.2(b) which includes data for all four samples. Excluding the data for sample A which has a MoGe layer only 6 nm thick and hence an incomplete superconducting transition due to the limitation on the lowest available temperature of 2 K, the experimental results on other samples follow the theoretical prediction nicely. We obtained fitting parameters Δ_0 = 2300 K, 800 K, and 250 K and T_{c0} = 4.70 K, 4.33 K, and 3.05 K for the networks of 20 nm, 15 nm and 10 nm thick, respectively. For an individual nanowire with length L, $\Delta_0 \approx 0.83\frac{L}{\xi_0}\frac{R_Q}{R_N}T_{c0}$ where R_Q =

6.45 kΩ is the quantum resistance and R_N is the normal state resistance.[39] The values of Δ_0 obtained from fitting the $R(T)$ curves were about 1/3 of those calculated with the experimentally determined L, R_N and T_{c0} of the nanowires.[39] In our multiply connected networks, the length L is not well defined. However, assuming all samples have similar L, we can estimate the ratios of Δ_0 with the experimental values of T_{c0}/R_N. The calculated ratio (~5:3:1) using R_N = 534, 806, 1729 Ω for the networks with 20, 15 and 10 nm thickness is within a factor of 2 from that (~9:3:1) derived by fitting the $R(T)$ curves with Eq.(3).

The above results indicate that the MoGe sections between neighboring holes behave like individual 1D nanowires. That is, all of our samples can be treated as networks of 1D nanowires. This is understandable since the temperature dependent superconducting coherence length $\xi(T) = \xi_0(1 - T/T_{c0})^{-1/2}$ with $\xi_0 = 8$ nm[5,39] is larger than the widths w of the MoGe sections between neighboring holes in the experimental temperature range for all samples. In fact, due to the divergent nature of $\xi(T)$ as T approaches T_{c0}, any perforated superconducting film, with small enough w, should behave as a network of 1D nanowires within a certain temperature range near T_{c0}.[40,41] The reduction in w helps to extend this temperature range. According to the criterion of $w \leq 1.84\xi(T)$ for defining 1D confinement, all our four samples should behave as networks of 1D nanowires at any experimentally accessible temperature below T_c.

In doubly connected thin superconductors, such as hollow cylinders[38,42] and loops[43,44] where the thickness of the wall and the line width of the loop are comparable to the superconducting coherence length, the fluxoid is known to be quantized. The quantization leads to a periodic oscillation in the magnetic field dependence of the critical temperature due to the field dependent velocity of the confined Cooper pairs. This Little-Parks effect[42] also occurs in a network of 1D superconducting nanowires. The Little-Parks effect[42] and the 1D confinement of 'Cooper pairs'

arising from the multiply connected hole-array are inextricably linked, destroying the 2D behavior normally expected of a thin film. For example, the *H-T* phase diagram of a continuous 2D film in perpendicular magnetic fields and at temperature not far away from T_{c0} follows a linear relationship $H_{c2} = \Phi_0 / [2\pi\xi^2(T)] = \Phi_0(1 - T/T_{c0}) / 2\pi\xi_0^2$,[45] where $\Phi_0 = hc/2e = 20.7\text{G}\bullet\mu\text{m}^2$ is the flux quantum. On the other hand, a superconducting film containing an array of holes at temperatures near T_{c0} usually have a phase diagram with an oscillatory variation superimposed on a parabolic background $H_{c2} = \sqrt{12}\Phi_0 / [2\pi w\xi(T)] = \sqrt{12}\Phi_0(1 - T/T_{c0})^{1/2} / 2\pi w\xi_0$.[45] This is consistent with the above discussions on the dimensionality change in a perforated film due to the temperature dependence of the coherence length. The parabolic relation for the *H-T* phase diagram has been in fact experimentally verified in 1D Nb nanowires.[22]

In order to determine the *H-T* phase diagram of our samples, we measured *R*(*T,H*) curves at small constant currents and various fixed magnetic fields. The data for sample D with magnetic fields up to 7 Tesla are presented in Fig.3(a). Notably, the superconducting transition shifts in an essentially parallel fashion in magnetic fields higher than 2 Tesla. That is, the applied magnetic fields affect only the critical temperature while causing negligible dissipation, for example, from the motion of magnetic flux lines. The relevant *H-T* phase diagrams defined with various resistance criteria are given in Fig.3(b). As can be seen directly in the inset which presents the data in the form of H^2 versus *T*, the phase diagram at high fields indeed follows $H_{c2} \sim (1 - T/T_{c0})^{1/2}$, as expected for a network of 1D nanowires[41,45] and contrasts to that of the 2D reference film as given in the inset of Fig.3(a). The shift in T_c to lower values from the parabolic background at magnetic fields less than 1 Tesla can be attributed to the T_c suppression due to the Little-Parks effect. Although the decrease in the amplitude of the T_c suppression at a higher resistance criterion is not straightforwardly

understandable, it is consistent with previous observations including the original experiment by Little and Parks.[42] Such a dissipation level dependent T_c suppression can cause the $R(T)$ curves in Fig. 3(a) (for $H < 2.0$ T) to cross one another .

In a regular network of 1D nanowires, the contribution from the Little-Parks effect causes T_c to oscillate with a magnetic field period of $H_0 = \Phi_0 / S$ where S is the area of the unit cell of the array. By using the nominal diameter of 20 nm and ~10 nm for the section between neighboring holes, the estimated H_0 for our samples is ~2.6 T, assuming the holes are distributed in a triangular lattice which is the most favorable arrangement of self-assembled objects. However, no anomaly can be identified at magnetic fields around 2.6 Tesla in the phase diagram in Fig.3(b). Instead, the values of the T_c at 1.2 Tesla and 1.4 Tesla are slightly larger than those of the surrounding fields. Although it was reported that the amplitude of the T_c oscillation decreases at high fields,[45] the experimental data points which are 0.5 Tesla apart in the *H-T* phase diagram of Fig.3(b) might not be dense enough to resolve an anomaly at high fields. Since an anomalous $T_c(H)$ oscillation in the phase diagram should be reflected in the magnetoresistance data, we obtained $R(H)$ curves at fixed temperatures using a finer ΔH interval. Data on the magnetoresistances of all four samples are presented in Fig.4. Aside from those for sample A which cannot complete its superconducting transition at the lowest achievable temperature of 2 K, the $R(H)$ curves of the other samples display a minimum in the field range of 1.2-1.5 T with decreasing temperature. Similar to the *H-T* phase diagram presented in Fig.3(b), the $R(H)$ curves also show no anomaly at fields around $H_0 = 2.6$ T.

The field values of 1.2-1.5 T are very close to half of the estimated oscillation period $H_0 = 2.6$ T based on the nominal pore diameter of 20 nm and the experimentally determined widths of the sections between neighboring pores. Thus, the anomalies in both the *H-T* phase diagram and the

$R(H)$ curves could originate from the fractional fluxoid quantization effect which occurs at fractional numbers (i.e. at $H_\alpha = \alpha H_0$ with α a fractional number) of the flux quantum per unit cell, as reported in other nanowire networks:[40] the Little-Parks effect induces a larger T_c suppression and stronger dissipation at fields around $H_0/2$, resulting in the observed resistance minimum. However, anomalies such as resistance minima induced by the Little-Parks effect are typically weaker at half flux quanta than that for integer flux quanta per unit cell.[41] The sole appearance of the anomaly at 1.2-1.5 T indicates that it most likely originates from the Little-Parks effect at the first integer flux quantum. These magnetic field values correspond to pore diameters of 26-29 nm. Although they are larger than the nominal diameter of 20 nm claimed by the manufacturer, the derived sizes are reasonably within the experimental error in determining such small dimensions. Furthermore, the pores, as can be seen from the SEM micrographs in Fig.1, are not circular. Since the smallest dimension of the pores is the determining factor for the filtration purpose, the actual pore area can indeed be larger than that estimated assuming a circle with the smallest filtration dimension as the diameter.

Nanoporous membranes, e.g. anodic aluminum oxide (AAO) have been pursued as substrates for introducing vortex pinning centers of high density into superconducting films.[45-48] Commensurate vortex pinning, i.e. when an integer number of flux quantum, is commensurate with the unit-cell of the hole-array superconductor, can also induce similar anomalies in the magnetoresistance as those expected from the Little-Parks effect.[41] One way to distinguish them is to probe the dissipation of a nanoporous superconducting film in various magnetic field orientations.[41] In the commensurate pinning scenario, the holes serve only as pinning centers for the vortices but do not change the 2D nature of the film. As predicted by the Tinkham formula[1] and confirmed by experiments in Nb films[22] the critical field of a 2D film becomes larger when the magnetic field is tilted towards the

film surface ($\theta = 90°$). Accordingly, the dissipation is expected to decrease. This is in fact observed in our reference MoGe films on Si substrate, as can be seen from data presented in Fig.5(a) for the 20 nm thick sample. The angular dependence of the magnetoresistance for the associated MoGe network formed on filtration membrane is given in Fig.5(b). The difference with Fig.5(a) is evident: the resistances in parallel fields ($\theta = 90°$) higher than 2.5 T can be even larger than those in the perpendicular orientation ($\theta = 0°$). The $R(H)$ curves which were taken with a smaller field interval for these two field orientations are presented in Fig.6. A crossing of the two curves can be identified at a field below but close to 2 T, consistent with the data in Fig.5(b). More importantly, the network approaches the normal state earlier in parallel fields. That is, the critical field in parallel orientation is smaller, contrary to that predicted for a 2D film from the Tinkham formula.[1] On the other hand, the data in Fig.5(b) and Fig.6 can be consistently explained by invoking the 1D nature of the nanowires in the network: the thickness of the MoGe nanowires is expected to be larger than the width when a MoGe layer with nominal thickness of 20 nm is deposited onto the ~10 nm wide sections between pores in the filtration membrane, though the actual thickness may be less than 20 nm. Since the critical field of a 1D nanowire is inversely proportional to its transverse dimension exposed to the field,[1,22] it will have a smaller value in parallel orientation when the thickness is larger than the width. The larger dissipation at low magnetic fields in the perpendicular orientation is induced by the additional T_c suppression due to the Little-Parks effect. With reduction of the thickness of the deposited MoGe layer, the thickness of the nanowires should approach and eventually become smaller than the width, leading to the disappearance of the crossing in the $R(H)$ curves in the parallel and perpendicular field orientations. This trend is in fact verified by the data given in the inset of Fig.6 for the MoGe network with a nominal thickness of 10 nm. Since the thickness and width of the nanowires are close, the network has comparable dissipation at high

fields in both orientations while the Little-Parks effect induces much larger resistance at low perpendicular fields.

IV. CONCLUSIONS

We sputtered-deposited superconducting MoGe thin layers of various thicknesses onto commercially available filtration membranes containing dense nanopores with nominal diameter of 20 nm and width of ~10 nm for the section between neighboring pores. Resistivity measurements revealed that the temperature and current dependences of the dissipations in these samples could be understood with the dissipation mechanism expected for individual 1D superconducting nanowires, i.e. thermally activated phase slips. We also observed oscillations attributable to the Little-Parks effect in both the *H-T* phase diagram and the magnetoresistance curves. These results, along with the comparisons of magnetoresistances in various magnetic field orientations and the estimated coherence length with the width of the superconducting section between neighboring holes, allow us to conclude that our perforated MoGe layers deposited onto the nanoporous filtration membrane substrates are in fact networks of 1D superconducting MoGe nanowires. Since such networks exhibit physical properties of individual 1D nanowires while can be fabricated easily, our fabrication approach can provide an alternative but more accessible templating method to achieve samples for exploring phenomena in superconductors with transverse dimensions down to few nanometers. The pores with diameter of ~20 nm in the substrate also enable us to conveniently fabricate multiply connected 1D superconductor with hole-diameter comparable to its zero-temperature coherence length, divulging the behavior of such extreme systems. Furthermore, our results also set limitations on efforts to pursue high commensurate vortex pinning fields by increasing the density of holes in a perforated film:[45-48] a reduction in the width of superconducting section between neighboring holes will increase the temperature range in which the perforated film

behaves as a network of 1D nanowires which dissipate energy when conducting electricity due to thermal and possibly also quantum phase slippages, eliminating the desired pinning effect of the introduced holes.

ACKNOWLEDMENTS

This work was supported by DOE BES under Grant No. DE-FG02-06ER46334 (sample fabrication and imaging) and Contract No. DE-AC02-06CH11357 (resistivity characterization). The film deposition and morphological analysis were performed at Argonne's Center for Nanoscale Materials (CNM) and Electron Microscopy Center (EMC), respectively, which both are funded by DOE under contract DE-AC02-06CH11357.

*Corresponding author, xiao@anl.gov or zxiao@niu.edu

References

[1]. M. Tinkham, Introduction to superconductivity, McGraw-Hill, Inc (1996).

[2]. N. Giordano, Phys. Rev. Lett. **61**, 2137 (1988); Phys. Rev. B **41**, 6350 (1990).

[3]. N. Giordano and E. R. Schuler, Phys. Rev. Lett. **63**, 2417 (1989).

[4]. A. Bezryadin, C. N. Lau, and M. Tinkham, Nature **404**, 971 (2000).

[5]. C. N. Lau, N. Markovic, M. Bockrath, A. Bezryadin, and M. Tinkham, Phys. Rev. Lett. **87**, 217003 (2001).

[6]. M. L. Tian, J. G. Wang, J. S. Kurtz, Y. Liu, M. H. W. Chan, T. S. Mayer, and T. E. Mallouk, Phys. Rev. B **71**, 104521 (2005).

[7]. M. Zgirski, K. -P. Riikonen, V. Touboltsev, and K. Arutyunov, Nano Lett. **5**, 1029 (2005).

[8]. M. Zgirski and K. Yu. Arutyunov, Phys. Rev. B **75,** 172509 (2007).

[9]. M. Zgirski, K. -P. Riikonen, V. Touboltsev, and K. Yu. Arutyunov, Phys. Rev. B **77,** 054508 (2008).

[10]. K. Xu and J. R. Heath, Nano Lett. **8**, 136 (2008); *ibid* **8**, 3845 (2008).

[11]. U. Patel, Z. L. Xiao, A. Gurevich, S. Avci, J. Hua, R. Divan, U. Welp, and W. K. Kwok, Phys. Rev. B **80**, 012504 (2009).

[12]. K. Yu. Arutyunov, D. S. Golubev, and A. D. Zaikin, Phys. Rep. **464**, 1 (2008).

[13]. Y. Chen, S. D. Snyder, and A. M. Goldman, Phys. Rev. Lett. **103**, 127002 (2009).

[14]. A. V. Herzog, P. Xiong, and R. C. Dynes, Phys. Rev. B **58**, 14199 (1998).

[15]. D. Y. Vodolazov, F.M. Peeters, L. Piraux, S. Matefi-Tempfli, and S. Michotte, Phys. Rev. Lett. **91**, 157001 (2003).

[16]. A. Johansson, G. Sambandamurthy, D. Shahar, N. Jacobson, and R. Tenne, Phys. Rev. Lett. **95**, 116805 (2005).

[17]. Y. S. Hor, U. Welp, Y. Ito, Z. L. Xiao, U. Patel, J. F. Mitchell, W. K. Kwok, and G. W. Crabtree, Appl. Phys. Lett. **87**, 142506 (2005).

[18]. A. Rogachev, A. T. Bolinger, and A. Bezryadin, Phys. Rev. Lett. **94**, 017004 (2005).

[19]. F. Altomare, A. M. Chang, M. R. Melloch, Y. Hong, and C. W. Tu, Phys. Rev. Lett. **97**, 017001 (2006).

[20]. U. Patel, S. Avci, Z. L. Xiao, J. Hua, S. H. Yu, Y. Ito, R. Divan, L. E. Ocola, C. Zheng, H. Claus, J. Hiller, U. Welp, D. J. Miller, and W. K. Kwok, Appl. Phys. Lett. **91**, 162508 (2007).

[21]. A. Falk, M. M. Deshmukh, A. L. Prieto, J. J. Urban, A. Jonas, and H. K. Park, Phys. Rev. B **75**, 020501 (2007).

[22]. J. Hua, Z. L. Xiao, A. Imre, S. H. Yu, U. Patel, L. E. Ocola, R. Divan, A. Koshelev, J. Pearson, U. Welp, and W. K. Kwok, Phys. Rev. Lett. **101**, 077003 (2008).

[23]. M. L. Tian, J. Wang, Q. Zhang, N. Kumar, T. E. Mallouk, and M. H. W. Chan, Nano Lett. **9**, 3196 (2009).

[24]. M. Sahu, M.-H. Bae, A. Rogachev, D. Pekker, T.-C.Wei, N. Shah, P. M. Goldbart, and A. Bezryadin, Nat. Phys. **5**, 503 (2009).

[25]. A. Bezryadin and P. M. Goldbart, Adv. Mater. **22**, 1111 (2010).

[26]. P. Li, P. M. Wu, Y. Bomze, I. V. Borzenets, G. Finkelstein, and A. M. Chang, Phys. Rev. Lett. **107**, 137004 (2011).

[27]. D. S. Golubev and A. D. Zaikin, Phys. Rev. B **78**, 144502 (2008).

[28]. K. Yu. Arutyunov, Physica C **468**, 272 (2008).

[29]. J. S. Langer and V. Ambegaokar, Phys. Rev. **164**, 498 (1967).

[30]. D. E. McCumber and B. I. Halperin, Phys. Rev. B **1**, 1054 (1970).

[31]. J. -M. Duan, Phys. Rev. Lett. **74**, 5128 (1995).

[32]. J. E. Lukens, R. J. Warburton, and W. W. Webb, Phys. Rev. Lett. **25**, 1170 (1970).

[33]. A. Rogachev, T. -C. Wei, D. Pekker, A. T. Bollinger, P.M. Goldbart, and A. Bezryadin, Phys. Rev. Lett. **97**, 137001 (2006).

[34]. X. Q. Zeng, M. L. Latimer, Z. L. Xiao, S. Panuganti, U. Welp, W. K. Kwok, and T. Xu, Nano Lett. **11**, 262 (2011).

[35]. Z. L. Xiao, C. Y. Han, U. Welp, H. H. Wang, W. K. Kwok, J. M. Hiller, R. E. Cook, D. J. Miller, and G. W. Crabtree, Nano Lett. **2**, 1293 (2002).

[36]. X. Q. Zeng, Y. L. Wang, H. Deng, M. L. Latimer, Z. L. Xiao, J. Pearson, T. Xu, H. H. Wang, U. Welp, G. W. Crabtree, and W. K. Kwok, ACS Nano **5**, 7443 (2011).

[37]. W. A. Little, Phys. Rev. **156**, 396 (1967).

[38]. Y. Liu, Y. Zadorozhny, M. M. Rosario, B. Y. Rock, P. T. Carrigan, and H. Wang, Science **294**, 2332 (2001).

[39]. M.-H. Bae, R. C. Dinsmore III, T. Aref, M. Brenner, and A. Bezryadin, Nano Lett. **9**, 1889 (2009).

[40]. B. Pannetier, J. Chaussy, R. Rammal, and J. C. Villegier, Phys. Rev. Lett. **53**, 1845 (1984).

[41]. U. Patel, Z. L. Xiao, J. Hua, T. Xu, D. Rosenmann, V. Novosad, J. Pearson, U. Welp, W. K. Kwok, and G. W. Crabtree, Phys. Rev. B **76,** 020508 (R) (2007).

[42]. R. D. Parks and W. A. Little, Phys. Rev. A **133**, 97 (1964).

[43]. V. V. Moshchalkov, L. Gielen, M. Dhalle, C. Vanhaesendonck, and Y. Bruynseraede, Nature **373**, 319 (1995).

[44]. G. R. Berdiyorov, S. H. Yu, Z. L. Xiao, F. M. Peeters, J. Hua, A. Imre, and W. K. Kwok, Phys. Rev. B **80,** 064511 (2009).

[45]. U. Welp, Z. L. Xiao, J. S. Jiang, V. K. Vlasko-Vlasov, S. Bader, G. W. Crabtree, J. Liang, H. Chik, and J. Xu, Phys. Rev. B. **66**, 212507 (2002).

[46]. W. Vinckx, J. Vanacken, V. V. Moshchalkov, S. Matefi-Tempfli, M. Matefi-Tempfli, S. Michotte, L. Piraux, and X. Ye, Physica C **459**, 5 (2007).

[47]. P. Sabatino, C. Cirillo, G. Carapella, M. Trezza, and C. Attanasio, J. Appl. Phys. **108**, 053906 (2010).

[48]. C. Chiliotte, G. Pasquini, V. Bekeris, J. E. Villegas, C. -P. Li, and I. K. Schuller, Supercond. Sci. Technol. **24**, 065008 (2011).

Figure captions

FIG.1. Top-view scanning electron microscopy (SEM) micrographs of MoGe nanowire networks sputter-deposited on an Anodisc®13 alumina membranes with a nominal filtration pore diameter of 20 nm. The thicknesses of the deposited MoGe layers are 6 nm (a) for sample A, 10 nm (b) for sample B, 15 nm (c) for sample C, and 20 nm (d) for sample D, respectively. The scale bar is 200 nm.

FIG.2. (color online) (a) Current dependence of the voltage $V(I)$ for sample D atvarious fixed temperatures. The temperature interval between 4.3 K and 4.6 K is 50 mK. (b) Temperature dependence of the resistance $R(T)$ curves for all four samples at small constant currents (I = 1 μA for samples A, B and C, and I = 2 μA for sample D). The symbols are experimental data in both panels and the solid lines in (a) and (b) represent fits with TAPS model Eq.(2) and Eq.(3), respectively. No external magnetic field was applied during the measurements.

FIG.3. (color online) (a) $R(T)$ curves for sample D (t = 20nm) at a constant current (I = 2 μA) and in various magnetic fields. The magnetic field intervals for the presented data are 500G, 0.2T and 0.5T for magnetic fields in the range of 0-0.1T, 0.2-2T and 2.5-7T, respectively. (b) Critical temperature versus magnetic field $T_c(H)$ phase diagrams for sample D obtained with resistance criteria of 1%, 10% and 50% of the normal state resistance R_N. The same data are plotted in the inset as H^2 versus T to show the parabolic relation of $H \sim (1-T_c/T_{c0})^{1/2}$ expected of a 1D nanowire. The relevant $T_c(H)$ phase diagrams for the reference film of Sample D are given in the inset of (a).

FIG.4. (color online) Magnetic field dependence of the resistances $R(H)$ curves at various temperatures for samples with nominal thicknesses of t = 6 nm (a), 10 nm (b), 15 nm (c) and 20 nm (d) for the deposited MoGe layers. The temperature intervals in (c) and (d) are 0.1 K and 0.05 K, respectively.

FIG.5. (color online) (a) and (b) present the angular dependence of the magnetoresistances $R(\theta)$ for 20 nm thick MoGe deposited on a silicon substrate (Ref. Film) and a filtration membrane (network, Sample D), respectively. The orientation of magnetic field perpendicular to the Si substrate and the filtration membrane surface is defined as $\theta = 0°$.

FIG.6. (color online) Magnetic field dependence of the resistances $R(H)$ for Sample D (20 nm thick network) at 4.4 K and in perpendicular ($\theta = 0°$, open symbols) and parallel ($\theta = 90°$, solid lines) magnetic fields. Inset: $R(H)$ curves for Sample B (10 nm thick network) in both orientations of the magnetic field and at various temperatures.

FIG.1

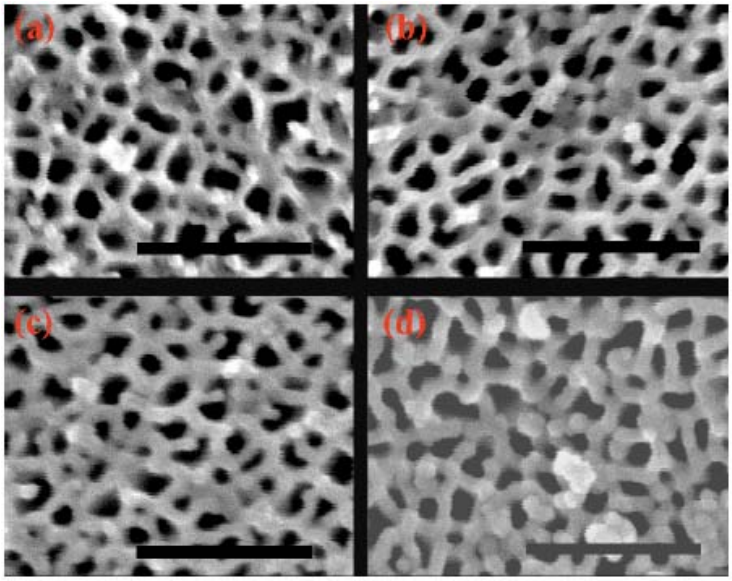

FIG. 2

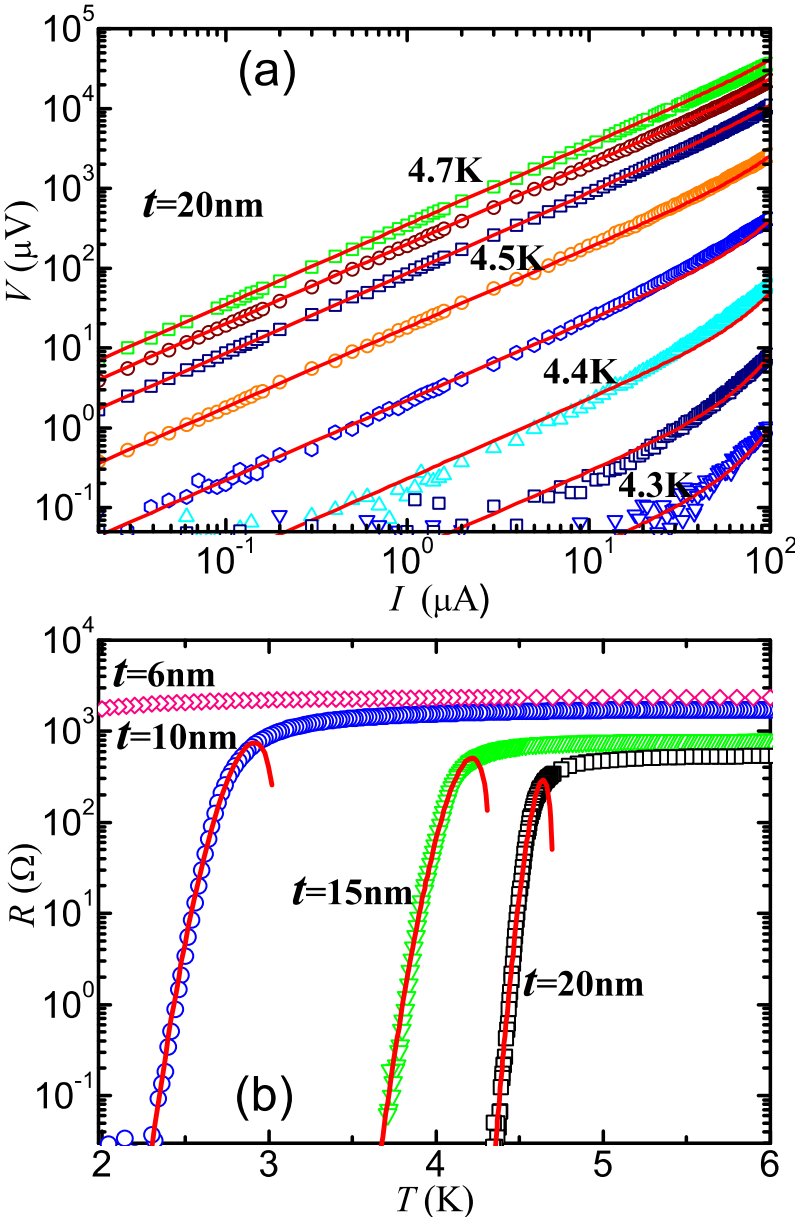

FIG. 3

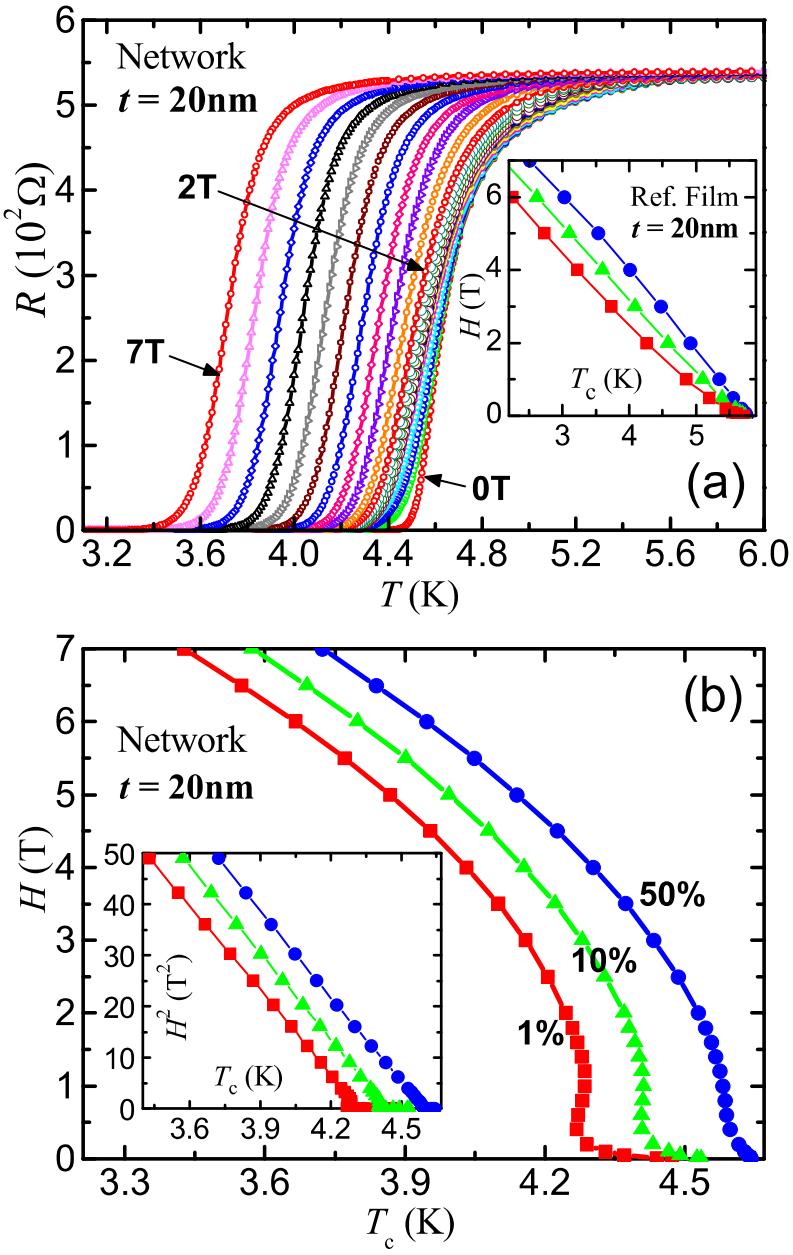
Network
t = 20nm
2T
7T
0T
R (10^2Ω)
T (K)
Ref. Film
t = 20nm
H (T)
T_c (K)
(a)
(b)
50%
10%
1%
H^2 (T^2)

FIG.4

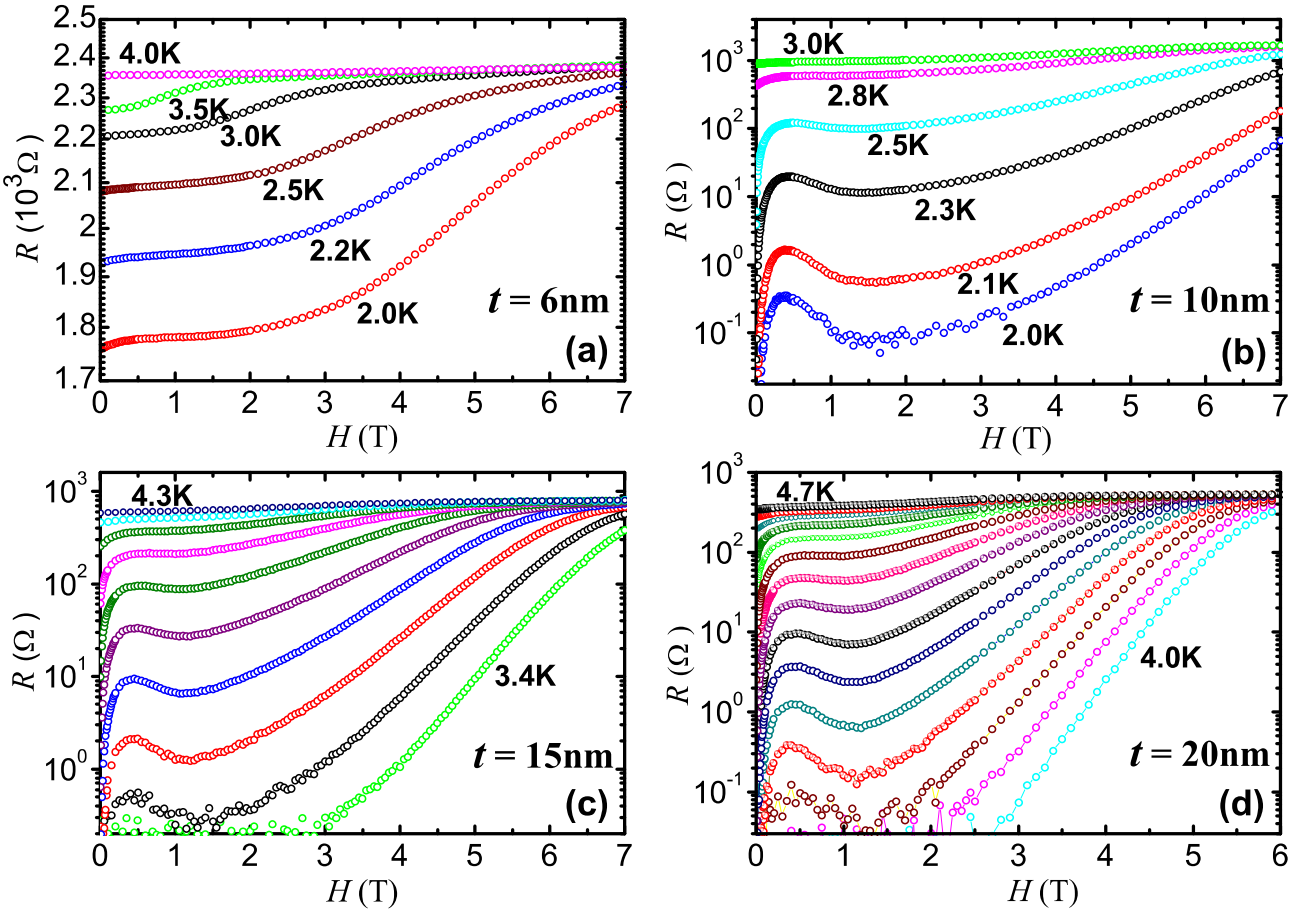
4.0K
3.5K
3.0K
2.5K
2.2K
2.0K
t = 6nm
(a)
R (10^3Ω)
H (T)
3.0K
2.8K
2.5K
2.3K
2.1K
2.0K
t = 10nm
(b)
R (Ω)
H (T)
4.3K
3.4K
t = 15nm
(c)
R (Ω)
H (T)
4.7K
4.0K
t = 20nm
(d)
R (Ω)
H (T)

FIG.5

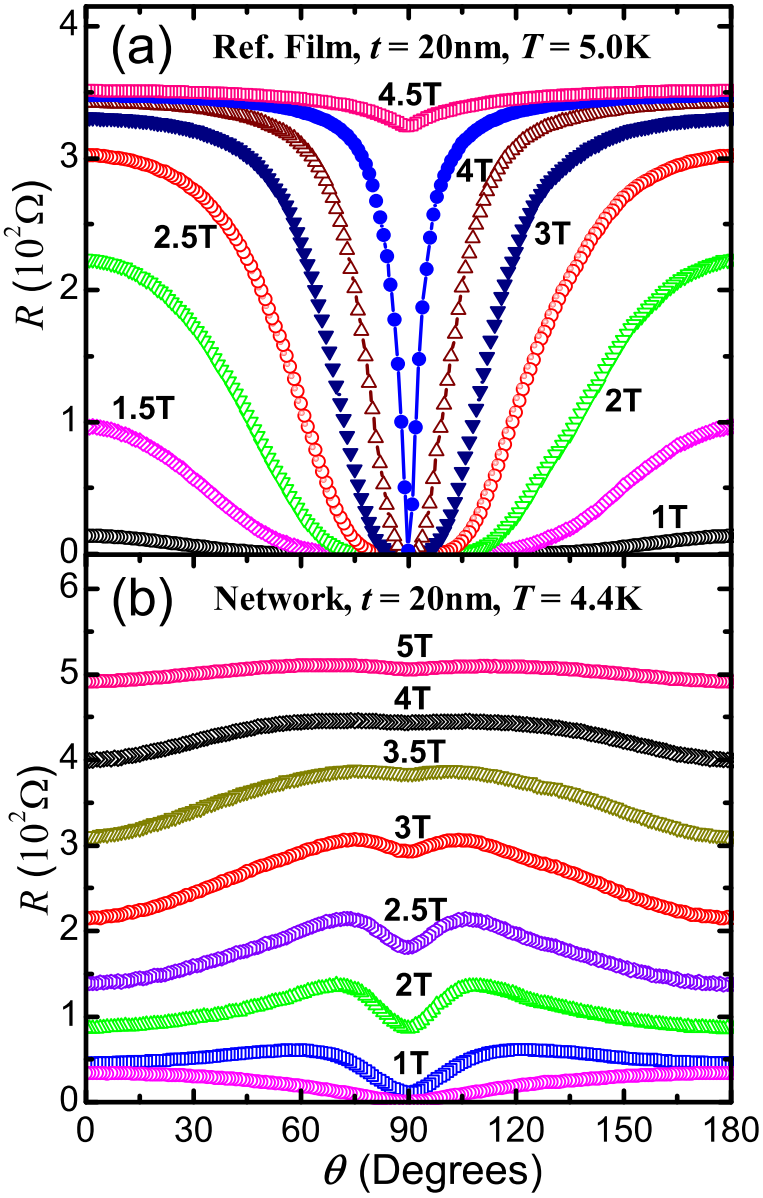
(a) Ref. Film, t = 20nm, T = 5.0K
4.5T
4T
3T
2.5T
2T
1.5T
1T
R (10^2Ω)
(b) Network, t = 20nm, T = 4.4K
5T
4T
3.5T
3T
2.5T
2T
1T
R (10^2Ω)
θ (Degrees)

FIG.6

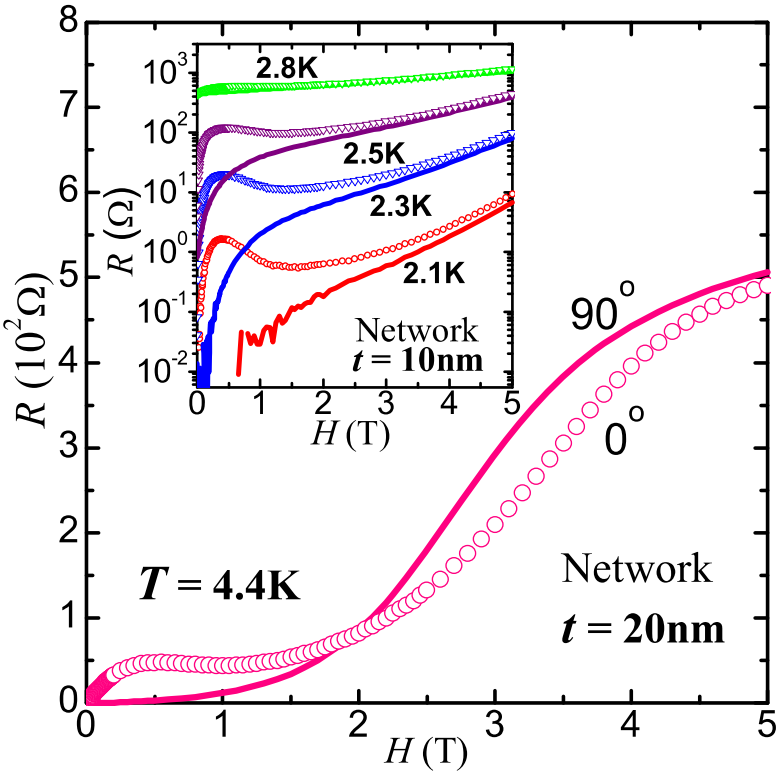
R (10^2Ω)
H (T)
T = 4.4K
90°
0°
Network
t = 20nm
R (Ω)
2.8K
2.5K
2.3K
2.1K
Network
t = 10nm